Genome Destabilizing Mutator Alleles Drive Specific Mutational Trajectories in *Saccharomyces cerevisiae*

Peter C. Stirling,*,[1,2] Yaoqing Shen,[†] Richard Corbett,[†] Steven J. M. Jones,[†] and Philip Hieter*,[2]
*Michael Smith Laboratories, University of British Columbia, Vancouver, BC, Canada V6T 1Z4, and [†]Michael Smith Genome Sciences Centre, Vancouver, BC, Canada V5Z 4S6

ABSTRACT In addition to environmental factors and intrinsic variations in base substitution rates, specific genome-destabilizing mutations can shape the mutational trajectory of genomes. How specific alleles influence the nature and position of accumulated mutations in a genomic context is largely unknown. Understanding the impact of genome-destabilizing alleles is particularly relevant to cancer genomes where biased mutational signatures are identifiable. We first created a more complete picture of cellular pathways that impact mutation rate using a primary screen to identify essential *Saccharomyces cerevisiae* gene mutations that cause mutator phenotypes. Drawing primarily on new alleles identified in this resource, we measure the impact of diverse mutator alleles on mutation patterns directly by whole-genome sequencing of 68 mutation-accumulation strains derived from wild-type and 11 parental mutator genotypes. The accumulated mutations differ across mutator strains, displaying base-substitution biases, allele-specific mutation hotspots, and break-associated mutation clustering. For example, in mutants of POLα and the Cdc13–Stn1–Ten1 complex, we find a distinct subtelomeric bias for mutations that we show is independent of the target sequence. Together our data suggest that specific genome-instability mutations are sufficient to drive discrete mutational signatures, some of which share properties with mutation patterns seen in tumors. Thus, in a population of cells, genome-instability mutations could influence clonal evolution by establishing discrete mutational trajectories for genomes.

EVOLUTIONARY analysis and laboratory studies show that mutation rates vary across chromosomes in unperturbed cells in association with factors such as base composition, repair efficiency, transcription, or replication timing (reviewed in Nishant *et al.* 2009). More recently, observations of mutation clustering in long stretches of single-stranded DNA (ssDNA) have been posited as conserved mutational mechanisms operating in tumors and methylmethane sulfonate (MMS)-treated yeast cells (Roberts *et al.* 2012). However, the influence of specific mutations on mutational patterns in the genome is usually not well characterized. Nonetheless, the spectrum of mutations will strongly influence the rates at which important phenotypes evolve. Recent work in *Escherichia coli* nicely demonstrates this concept by showing that different mutator alleles more potently adapt to different antibiotics based on the penetrance of the resistance mutations conferred by each mutator (Couce *et al.* 2013). A handful of studies in models such as *Caenorhabditis elegans* and *Saccharomyces cerevisiae* have linked mutator alleles to mutation patterns on a genome-wide scale (*e.g.*, *dog-1* deficiency mutating G-quadruplexes, mismatch-repair-deficiency mutating homopolymers, DNA polymerase δ variants preferentially mutating lagging strands) (Cheung *et al.* 2002; Larrea *et al.* 2010; Zanders *et al.* 2010). However, the influence of most mutator alleles on mutation patterns is not understood at this level. Thus, not only the mutation rate increase conferred by a mutator allele, but also its unique mutational signature (*i.e.*, preferred type of mutation and bias to a genomic context, if any) generates its effect on genome stability and evolution.

Tumor genomes accumulate alterations during oncogenesis. The accumulation of mutations, aneuploidies, or epigenetic changes frequently exceeds the normal rate of such events due to a predisposing mutation or environmental

doi: 10.1534/genetics.113.159806
Manuscript received November 15, 2013; accepted for publication December 4, 2013; published Early Online December 13, 2013.
Available freely online through the author-supported open access option.
Supporting information is available online at http://www.genetics.org/lookup/suppl/doi:10.1534/genetics.113.159806/-/DC1.
[1]Present address: Terry Fox Laboratory, British Columbia Cancer Agency, Vancouver, BC, Canada V5Z 1L3.
[2]Corresponding authors: Terry Fox Laboratory, BC Cancer Agency, 675 West 10th Ave., Vancouver, BC, Canada V5Z1L3. E-mail: pstirling@bccrc.ca; and Michael Smith Laboratories, University of British Columbia, 2185 East Mall, Vancouver, BC, Canada V6T 1Z4. E-mail: hieter@msl.ubc.ca

state that increases genetic instability. This in turn acts as an enabling characteristic of oncogenesis in most tumors (Hanahan and Weinberg 2011). Increased genetic instability, either in the form of increased mutation rate or chromosome instability (CIN), may promote selection of oncogenic cells from pre-oncogenic populations by increasing the likelihood that the requisite constellation of oncogenic mutations will occur in fewer cell divisions (Stratton *et al.* 2009; Loeb 2011). Thus, early genome-destabilizing mutations have the potential to shape the evolutionary trajectory of precancerous cells and intratumoral heterogeneity in large tumor cell populations.

Analysis of tumor genomes has uncovered discrete mutational signatures operating within and between tumor types (Nik-Zainal *et al.* 2012; Alexandrov *et al.* 2013b). These powerful computational approaches have demonstrated that multiple mutational processes operate simultaneously in tumors (Nik-Zainal *et al.* 2012; Alexandrov *et al.* 2013a). Mutational signatures can result from environmental exposure to genotoxins such as ultraviolet light or components of cigarette smoke (Pleasance *et al.* 2010a,b). Other signatures show the signs of endogenous processes such as the inappropriate action of APOBEC family cytosine deaminases (Nik-Zainal *et al.* 2012; Alexandrov *et al.* 2013b; Burns *et al.* 2013). Indeed, APOBECs from various sources are sufficient to induce breast-cancer-like patterns of mutations (*i.e.*, clustered hypermutation of C:G basepairs or "kataegis") when expressed ectopically in yeast (Lada *et al.* 2012; Alexandrov *et al.* 2013b; Taylor *et al.* 2013). Importantly, mutant alleles in genome-stability factors such as the DNA repair proteins BRCA1 and BRCA2 also correlate with a characteristic pattern of mutations (Nik-Zainal *et al.* 2012).

Screens in yeast have identified dozens of genome-destabilizing "mutator" alleles that function in a handful of cellular pathways (Huang *et al.* 2003; Smith *et al.* 2004). However, these efforts have focused on nonessential gene deletions available from the yeast knockout collection and thus are missing the fraction of mutators encoded by essential genes. In this study we probe mutant alleles of >500 essential yeast genes for those that increase the forward mutation rate, highlighting the role of the DNA replication machinery in suppressing mutation accumulation. Analyzing whole genome sequences for 68 mutation accumulation lines derived from 12 parental genotypes, reveals examples of mutator-allele-associated base-substitution biases, clustered mutations, and locus-specific patterns of mutations. These observations show that different genome destabilizing lesions can result in discrete mutational trajectories for a genome and thus, for a population of cells, could influence clonal evolution.

Materials and Methods

Yeast growth, microscopy, and fluctuation analyses

Strains used are listed in Supporting Information, Table S7. Yeast were grown on rich media except for *CAN1*, *URA3* fluctuation, or *LEU2* recombination analyses, which were conducted as described (Lang and Murray 2008; Stirling *et al.* 2012). Rates per generation were calculated from at least 12 (recombination rate) or 18 (mutation rate) independent cultures using the FALCOR program (Hall *et al.* 2009). For microscopy, logarithmic cultures in synthetic medium were shifted to 37° for 2 hr mounted on concanavalin-coated slides, imaged using Metamorph (Molecular Devices), and scored using ImageJ (rsbweb.nih.gov/ij/) as described (Stirling *et al.* 2012).

Mutation accumulation

Overnight cultures of parent clones were diluted into parallel cultures in 96 DeepWell plates. Cultures saturated over 3 days were diluted 10,000-fold in fresh medium and the process was repeated until ~195 generations elapsed. Temperature sensitivity (ts) was confirmed by spot assays at 37° for the ts-alleles to remove wells with revertants. For evolved wild type (WT), *rad52*Δ, *tsa1*Δ, and ts-wells, single colonies were isolated and genomic DNA was prepared using two rounds of phenol-chloroform extraction and ethanol precipitation with an intervening RNaseA step (75 μg/ml RNaseA at 37°, 30 min).

Sequencing, data analysis, and mutation identification

Whole-genome sequencing was done using the Illumina HiSeq2000 platform. Sequence files are deposited at the National Center for Biotechnology Information (NCBI) Sequence Read Archive (http://www.ncbi.nlm.nih.gov/sra) (no. PRJNA219315). After whole-genome sequencing on 12 parental strains and 4–6 evolved progeny strains, postquality control reads were aligned to the *S. cerevisiae* reference genome (University of California Santa Cruz version sacCer2) using Burrows-Wheeler Aligner 0.5.7 (Li and Durbin 2009), using default parameters. For each pair of parent–progeny, joint variant calling was carried out using SAMtools 0.1.13 utilities (Li *et al.* 2009), with the parameters −C50 to decrease false calls from reads with excessive mismatches to the reference. A score based on log ratio of genotype likelihoods was used to identify variants in the progeny, with a threshold of 20 (Li *et al.* 2009). Positions of variants determined in the parental strains were ignored in our analysis regardless of their quality score to reduce false positive calls. The remaining variants were annotated with SnpEff 3.0 (Cingolani *et al.* 2012), using the Ensembl sacCer2.61 database (Flicek *et al.* 2013). Copy-number variants were detected using a modified version of CNAseq developed at the Michael Smith Genome Sciences Centre, as described (Shah *et al.* 2006; Jones *et al.* 2010). As an additional quality control, we manually checked variants with Phred-scaled variant quality scores <20 using the Integrated Genomics Viewer (Broad Institute) and discarded those with poor read support.

Base substitution and flanking nucleotide bias

Base substitution biases were calculated using the Fisher exact test to compare with a wild-type mutation spectrum

derived from the literature (Lynch *et al.* 2008; Lang *et al.* 2013). As in the literature, each mutation, regardless of strand, is expressed as a change originating in a C or T (Nik-Zainal *et al.* 2012). A Holm–Bonferroni approach was applied to Fisher's test *P*-values to correct for multiple hypothesis testing; corrected *P*-values are reported.

Mutation clustering analysis

Clustering was assessed essentially as described (Roberts *et al.* 2012). Intermutation distances for variants in the genome of a single isolate were calculated and those appearing within a 100-kb window were tested statistically. For the purposes of this analysis, mutations within 10 bp were considered "complex mutations" and treated as a single event, thus not constituting clusters unto themselves. Using the intermutation distance (*i.e.*, cluster size) in base pairs, the number of mutations observed in a candidate cluster and the probability of finding a mutation at a given location in the genome, we calculated the cumulative probability on a negative binomial distribution of observing the intermutation distance at random. The probability of identifying a mutation at a given location was determined by dividing the total number of mutations (n) for a particular genotype by the number of base pairs sequenced for that strain (no. of genomes sequenced $\times$ 12,162,995 bp). Calculations were done using MatLab V7.12.0.635. To account for multiple hypothesis testing, we divided our original significance threshold ($P < 0.01$) by the number of putative clusters analyzed (103), establishing a corrected significance threshold of $P < 9.7 \times 10^{-5}$.

Results and Discussion

Systematic identification of mutator alleles in essential genes

Our previous efforts to catalog yeast CIN genes revealed a bias toward essential genes; thus we reasoned that there were likely to be unrecognized essential genes operating to suppress mutations. We surveyed 813 alleles in 525 essential genes (~50% of total) (Ben-Aroya *et al.* 2008; Breslow *et al.* 2008; Li *et al.* 2011) for increased *CAN1* mutation frequencies, identifying 47 mutator alleles in 38 genes (Figure 1A). Only those alleles that retested as mutators across five independent patches are included (Table S1). To assess the sensitivity of our assay, we quantified mutation rates for alleles of 33 mutator genes (Figure 1B). Fluctuation analysis revealed that all but two alleles had a twofold or higher increase in mutation rate at 30°, suggesting that our primary screen was as sensitive to changes in mutation rate as previous screens and that our retesting effectively removed false positives (Huang *et al.* 2003).

Combining our dataset with the *Saccharomyces* Genome Database phenotype term "mutation frequency: increased," we compiled the list of yeast genes with reported mutator phenotypes (Table S1). These 127 genes represent a community survey of >5000 yeast genes (~85% of total) for mutator phenotypes, thus most cellular pathways that suppress mutations are probably represented. Functional enrichment analysis of the mutator alleles highlights the dominant role of the DNA repair and replication machinery in suppressing mutations (Figure 1C). Gene Ontology analysis showed that essentially all DNA repair pathways are significantly enriched (*i.e.*, $P < 10^{-8}$ for base-excision repair, nucleotide excision repair, mismatch repair, break-induced replication, homologous recombination, and nonhomologous end joining). Nearly 90% of the mutators likely function at least partially in the nucleus, consistent with more direct mechanisms in preventing a mutator phenotype compared with CIN, for which ~40% of CIN genes function outside the nucleus (Stirling *et al.* 2011). Mutants affecting the nucleotide pool, oxidative stress response, or mitochondrial function make up the only nonnuclear functional groups, consistent with the established potential for these pathways to influence nuclear genome integrity indirectly through their effects on oxidative base damage and Fe-S cluster formation (Huang *et al.* 2003; Veatch *et al.* 2009). A total of 72 of 127 mutator alleles compiled here also have a reported CIN phenotype, highlighting the considerable overlap of the two phenotypes. Nonetheless, this list of essential mutator alleles enhances the resource of genome-destabilizing mutations available in yeast.

Determining the mutation spectra driven by different mutator alleles

The *CAN1* marker used as a primary screen for mutator alleles has been sequenced extensively to describe the mutational spectrum of mutator alleles (Huang *et al.* 2003). However, *CAN1* only tests mutations in ~1.8 kb of the ~12-Mb yeast genome and isolating CAN^r strains requires loss-of-function mutations, biasing the mutation spectrum toward frameshifts, stop codons, and a subset of amino acid substitutions. Therefore, it is plausible that different mutator alleles will selectively drive mutation in the genome based on a set of parameters that may or may not be represented in *CAN1*. A well-characterized example of this phenomenon is the association of mismatch repair deficiency with increased mutation rates in homopolymeric or microsatellite sequences (Zanders *et al.* 2010). Thus, while *CAN1* is a convenient marker for identifying mutator alleles, analysis of diverse sequence contexts is more likely to reveal any allele-specific locus biases that exist.

To explore the mutational spectrum for diverse mutator alleles in a whole-genome context we devised a mutation accumulation experiment. Eleven mutator alleles were chosen for this analysis: two strong and well-characterized mutators from the literature, namely deletions of the homologous recombination protein *RAD52* and the peroxiredoxin *TSA1* (Huang and Kolodner 2005; Mortensen *et al.* 2009), and nine mutator alleles identified in our primary screen of essential genes (Figure 1). The alleles were chosen partly to represent diverse cellular pathways [*e.g.*, homologous

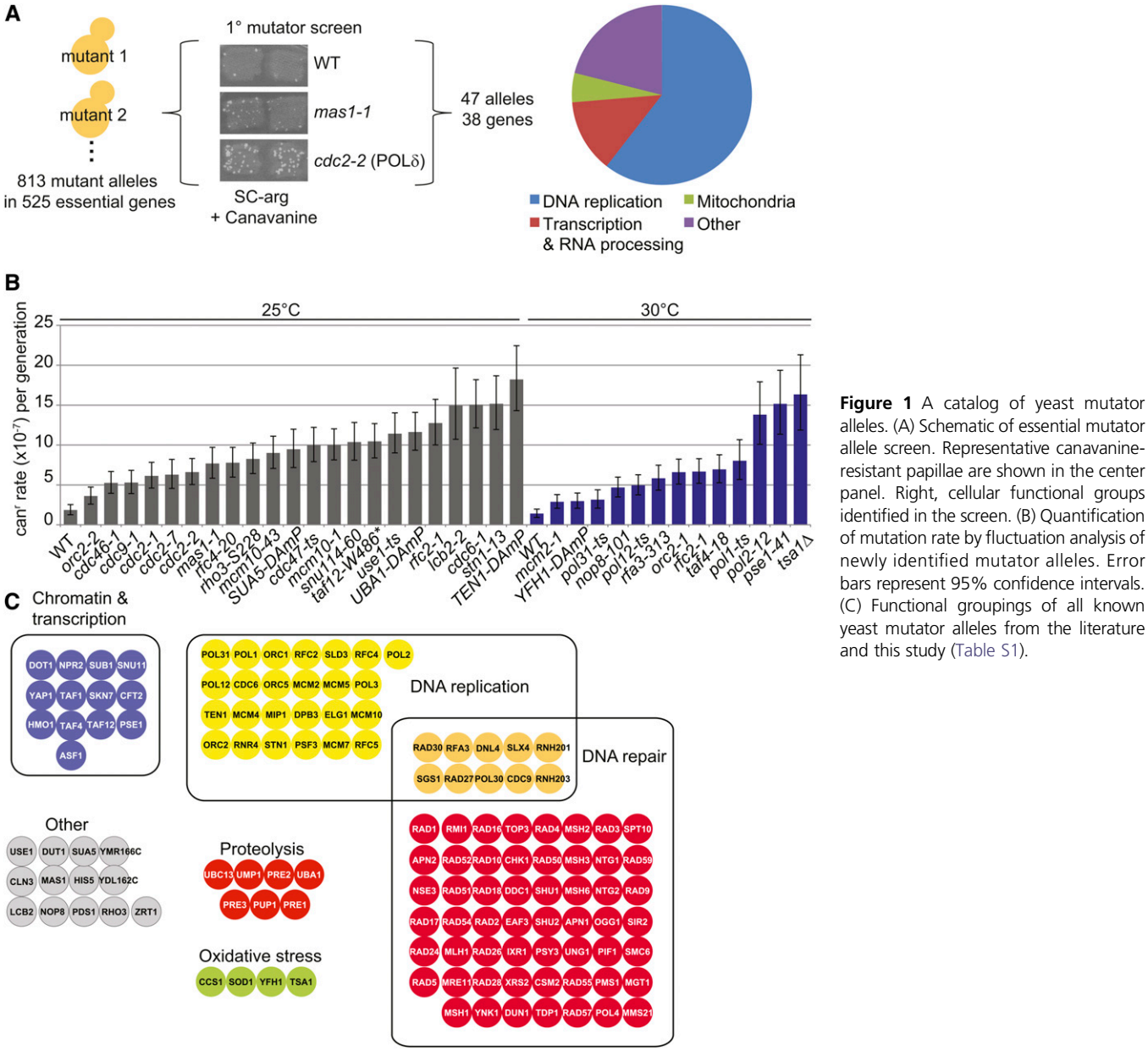

Figure 1 A catalog of yeast mutator alleles. (A) Schematic of essential mutator allele screen. Representative canavanine-resistant papillae are shown in the center panel. Right, cellular functional groups identified in the screen. (B) Quantification of mutation rate by fluctuation analysis of newly identified mutator alleles. Error bars represent 95% confidence intervals. (C) Functional groupings of all known yeast mutator alleles from the literature and this study (Table S1).

recombination (*rad52*Δ), oxidative stress tolerance (*tsa1*Δ), splicing (*snu114-60*), transcription (*taf12-W486**), mitochondrial function (*mas1-1*), and telomere capping (*stn1-13*)] and also acknowledge the inherent bias toward DNA replication by querying different perturbations in replication machinery (*i.e.*, *orc2-1*, *rfc2-1*, *mcm7-ts*, *pol1-ts*, and *pol2-12*). For each strain, a single parental clone was split into parallel cultures, grown for ~195 generations by repeated dilution, and single colonies were derived from the endpoint cultures. Genomic DNA from the parent and four to six independently evolved progeny was whole-genome sequenced for a total of 12 starting strain backgrounds, producing 80 haploid whole-yeast-genome sequences at an average of 57-fold sequence coverage (schematized in Figure 2A; Table S2). Subtracting the parental genotype from the evolved strains identifies accumulated variants. This experiment captured single-nucleotide variants (SNVs), copy-number variants (CNVs, *i.e.*, deletions or amplifications of large chromosomal regions), small insertion/deletion mutations (indels), and a few other types of chromosomal rearrangements (Figure 2B and Table S3). Based on published mutation rates (Lang and Murray 2008; Lynch *et al.* 2008), we predicted zero to two mutations per WT genome and observed a slightly higher but comparable rate (median = 2.5 mutations/genome; range, two to four mutations). In contrast, the mutator alleles produced ~2- to 10-fold more mutations on average (Figure 2B). SNVs were the most frequently identified mutation. One limitation of short read sequencing is difficulty in detecting indels between ~15 and 50 bp. However, the indels we did detect were

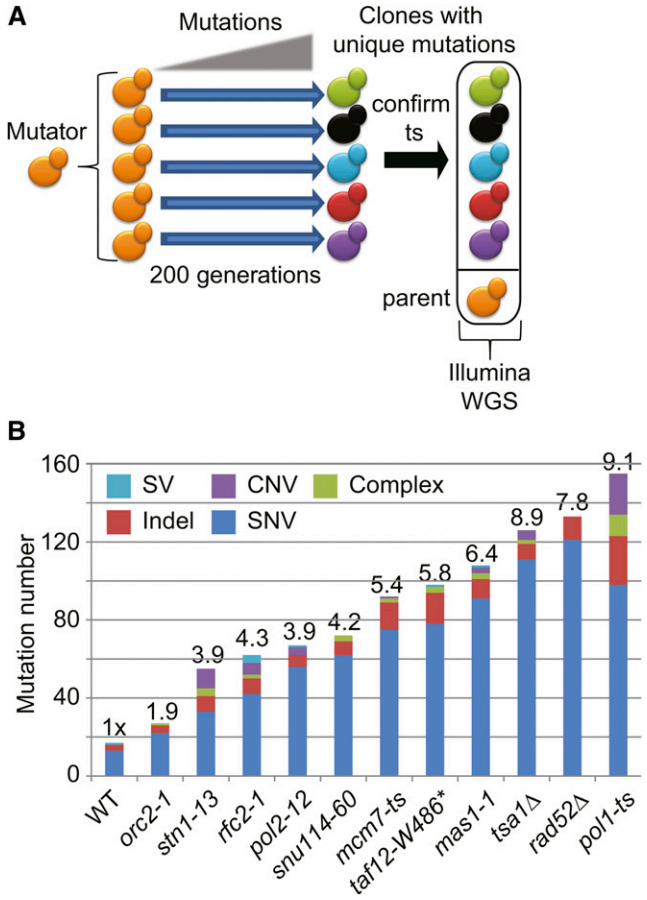

Figure 2 Determining the genomic mutation spectrum of mutator alleles. (A) Schematic of mutation accumulation experiment (see main text). Colors denote independent genomes. (B) Summary of mutations detected for mutator alleles. Fold increase in mutations/genome compared to WT are indicated above each bar. WGS, whole-genome sequencing; SV, structural variant; CNV, copy-number variant; SNV, single-nucleotide variant; indel, small insertion or deletion.

likely *bona fide* since the genomes of parents and evolved strains were compared relatively, using the same technology.

CNVs were not observed in the WT isolates but 7 of 11 mutator allele sets accumulated at least one predicted CNV during the experiment, including whole chromosome gains and segmental gains and losses (Table S3 and Table S4). Subtelomeric gains and losses were the most common type of CNV, presumably because large deletions in other parts of the genome would be lethal to a haploid cell and because telomeres represent repetitive, difficult-to-replicate regions prone to mutation (Nishant *et al.* 2010). Other types of structural variants were rarely detected but included large insertions, deletions, and inversions (Table S3 and Table S4).

Copy-number variants linked to hyperrecombination

In analyzing CNVs, we noted some common features of segmental changes internal to the chromosome. These CNVs were usually <20 kb, were invariably flanked by repetitive sequences (*e.g.*, *HXT6/HXT7* paralogues, *ENA1/ENA2/ENA5* paralogues, *RUF5-1/RUF5-2* ncRNAs, and Ty1 retrotransposons) and often contained an origin of replication. The nature of the CNVs indicated that unscheduled recombination events were likely taking place in these mutator strains, potentially linked to defective replication fork progression. Indeed some CNVs showed direct evidence of recombination (*e.g.*, homozygosity of *HXT6* and *HXT7* paralogues, Figure 3A) and others are known to be recombination hotspots (St Charles and Petes 2013). It is worth noting that additional events would almost certainly be evident in diploids where larger deletions or intrachromosomal rearrangements, lethal to the haploid cells in our experiment, could be tolerated.

Together these observations led us to hypothesize that many observed CNVs could be due to increases in homologous recombination. Using a plasmid-based assay for direct repeat recombination, we found that strains with the most segmental CNVs (*i.e.*, *stn1-13*, *pol1-ts*, and *tsa1*Δ) had significant increases in direct repeat recombination (Figure 3B). Consistently, several of these strains (*e.g.*, *POL1*, and *TSA1* mutants) have reported increases in Rad52 foci, indicative of ongoing DNA repair, whereas the Rad52 foci status of *stn1-13* is unknown (Ragu *et al.* 2007; Stirling *et al.* 2012). We scored a subset of mutator alleles from our screen for Rad52-YFP foci and found that *stn1-13*, along with other replication and transcription mutants, cause significant increases in Rad52 foci (Figure 3C and Table S1; Stirling *et al.* 2012). We suggest that some of the identified CNVs are driven by inappropriate recombination events due to increased DNA damage. While surprising for a circular plasmid given the role of Stn1 in telomere capping, the observed increase in plasmid-based recombination rate in *stn1-13* cells supports its recently described role in global DNA replication fork restart via interactions with the POLα complex (Stewart *et al.* 2012).

Varied base-substitution patterns originating in different mutator alleles

We pooled accumulated mutations for a given parental genotype to assess allele-associated mutation signatures. Variants were classified as originating in the pyrimidine base to simplify SNVs into six categories (*i.e.*, C to T or T to C transition and T to A, T to G, C to A, and C to G transversions) (Figure 4A and Table S5). Since we did not accumulate enough mutations in our WT strain to confidently set a baseline, we relied on the whole-genome and marker sequencing data compiled in the literature to set a standard of the yeast mutational spectrum (Figure 4B) (Lynch *et al.* 2008; Lang *et al.* 2013).

Even combining all the genomes sequenced for a given strain, we accumulated relatively few base changes for each strain and could not universally predict mutation biases. Previous studies with similar numbers of variants have focused on mutators that create very well-defined signatures (*e.g.*, indels in homopolymeric sequence for mismatch repair defects) (Zanders *et al.* 2010; Ma *et al.* 2012). Other studies have used strains with extremely high mutation rates due to

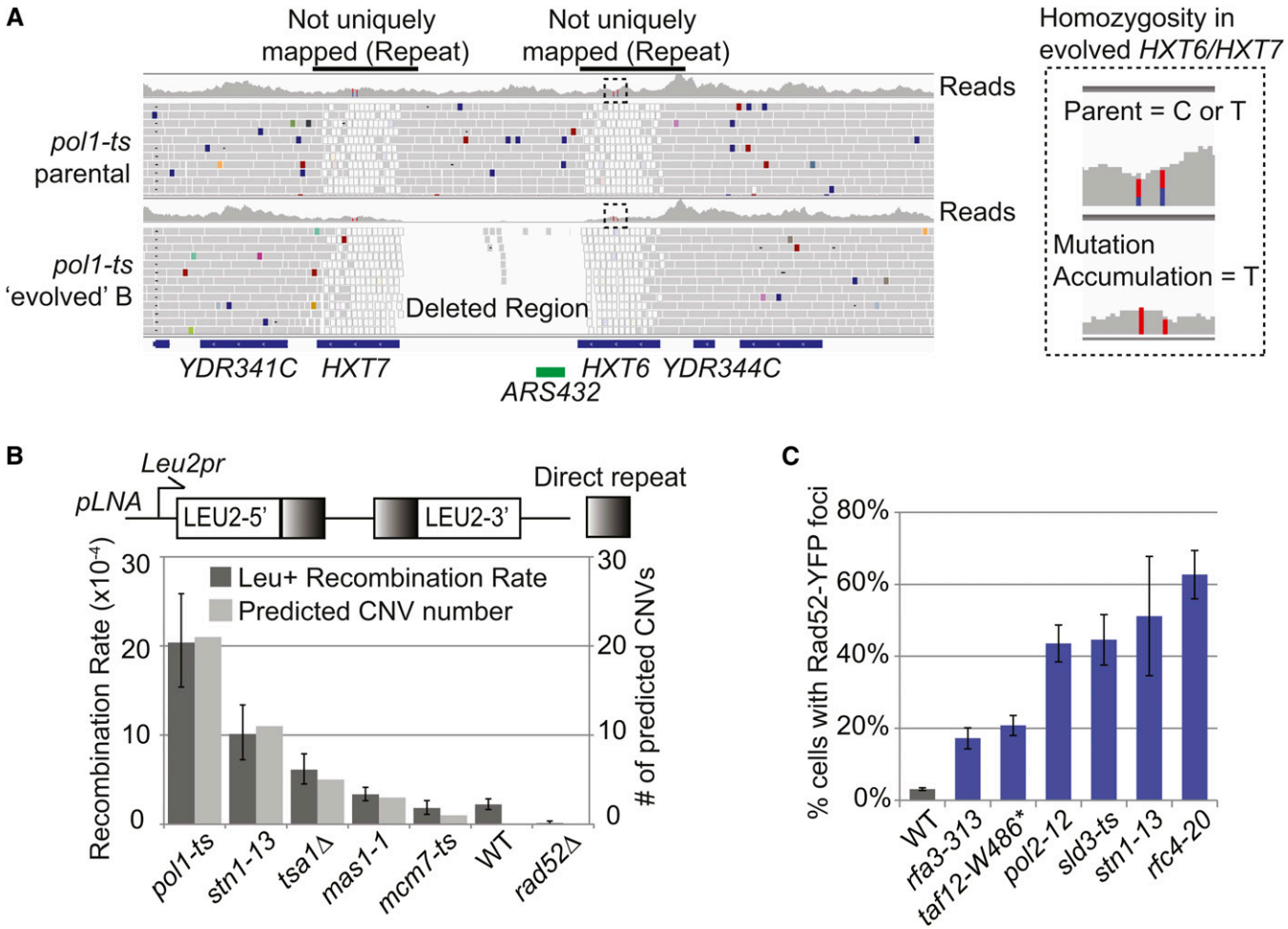

Figure 3 Linking segmental copy-number changes to recombination. (A) Example of segmental deletion in *pol1*-ts. Integrative Genomics Viewer of mapped reads shows a deletion encompassing ARS432, flanked by the *HXT6/HXT7* paralogues. Loss of sequence heterogeneity between *HXT6* and *-7* (dotted boxes) supports a deletion by intrachromosomal recombination. (B) Direct repeat recombination rates in selected mutator alleles. Error bars represent 95% confidence intervals. (C) Rad52-YFP foci accumulation in selected mutator alleles. Blue bars were significantly different from WT ($P < 0.01$). Error bars are the standard error of the mean.

multiple mutator alleles (Larrea *et al.* 2010). Remarkably, we did observe significant shifts in the observed mutation type for *rfc2-1*, *pol1-ts*, and *stn1-13* alleles using Fisher's exact test (Holm–Bonferroni corrected $P < 0.05$) (Figure 4B). *rad52*Δ exhibited candidate variation in the Fisher test but did not meet our significance threshold after correction for multiple hypothesis testing (Figure 4B). The driving force of mutation bias for *rfc2-1* and *stn1-13* appears to be a proportionate increase in transition frequency, while the spectrum of *pol1-ts* is more complex (*e.g.*, double the number of T to A transversions). Additional refinement and analyses of the context of base-substitution bias in such genome-wide studies will require larger numbers of variants and a continual refinement of the true WT mutation spectrum.

Limiting analysis to strains with >50 genic SNVs, we also observed a weak transcriptional strand bias in *rad52*Δ mutations (*i.e.*, increased C to T mutations in the transcribed strand), suggesting that inability to complete transcription-associated recombination may lead to an error-prone mechanism of repair in these cells (Figure S1). While we do not understand the mechanisms in each case, as has been seen in analysis of tumor genomes (Nik-Zainal *et al.* 2012), our data suggest that transcription could have a significant allele-specific influence on mutation spectra.

Regional and functional genomic elements dictate mutation position

Biased mutation position could reflect specific chromatin environments or functional features of the genome that interact with a mutator allele to drive mutations in a specific locus. Relationships with features such as transcription, nucleotide content, or replication timing have previously been noted in cancer and model organisms (Lang and Murray 2011; Drier *et al.* 2013). We first analyzed the relative position of mutations along the length of chromosomes irrespective of sequence features, normalizing mutation positions to the position along the chromosome from 0 to 100%. Kolmogorov–Smirnov tests showed that only the

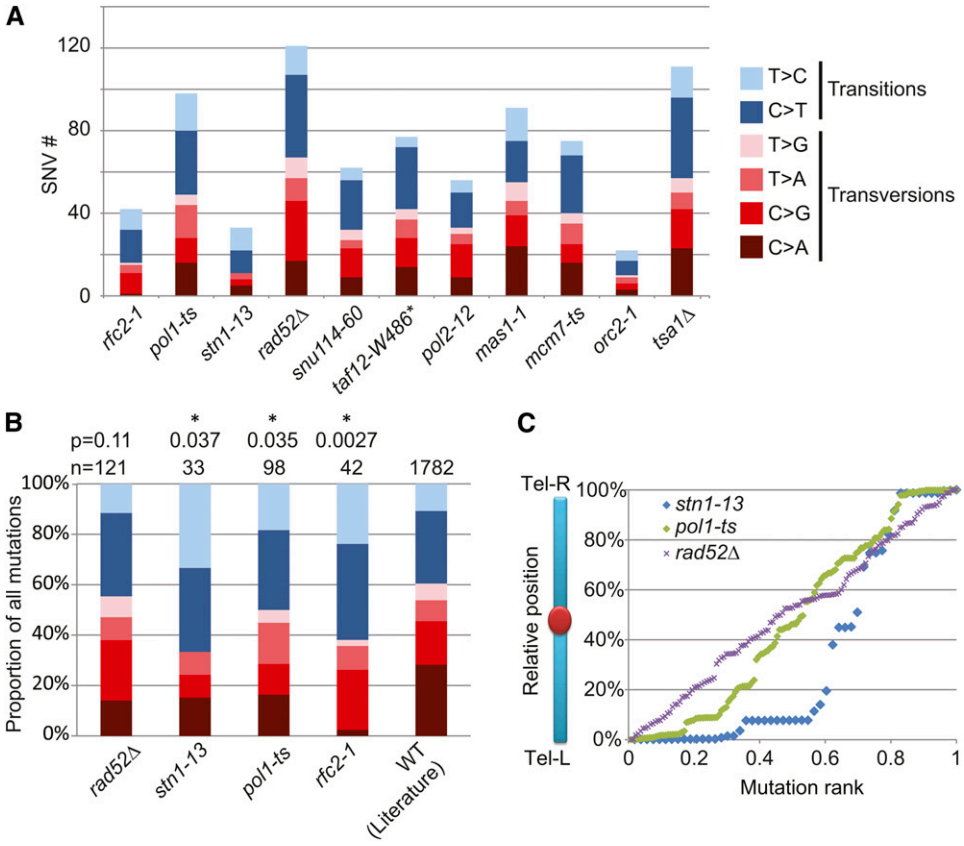

Figure 4 Mutator allele-driven biases in mutation type and position. (A) Base substitution types across mutator allele backgrounds. Shown are the raw number of each transversion (reds) and transition (blues) detected in the mutator genomes. (B) Proportion of mutation types. Selected data from A, expressed as a proportion, and its comparison with a WT spectrum (Lynch *et al.* 2008, 2013), reveal significant variations from the WT. *P*-values represent Holm–Bonferroni corrected results of a Fisher's exact test (*<0.05). (C) Mutation position as a percentage of chromosome length. Relative mutation position along the 16 chromosomes in *stn1-13* and *pol1-ts* differ significantly from *rad52Δ* (Kolmogorov–Smirnov $P < 0.05$). The *x*-axis (mutation rank) reflects the position of each mutation in an ordered list, expressed as a proportion of the total.

stn1-13 and *pol1-ts* mutation patterns differed significantly from an idealized distribution and from other alleles patterns (Figure 4C). The *stn1-13* and *pol1-ts* mutation profiles showed hotspots of mutation in subtelomeric regions not seen in other alleles. For *stn1-13* this bias was expected since previous work demonstrated that *stn1-13* cells accumulate ssDNA in telomeric regions (Grandin *et al.* 1997).

We investigated potential correlations between mutation position in a given mutator allele and a variety of functional features of the genome. Generally, we did not see significant associations with GC content or with transcribed regions of the genome. The one exception to this was for *stn1-13*, which showed increased mutations outside of genes, likely associated with mutation bias to gene-poor subtelomeres (Figure S2 and see below). Similar to observations in human evolutionary studies and in cancer genomes, we found that mutations in 5 of 11 mutators occur in regions with later average replication timing compared to the rest of the genome (Figure S2) (Raghuraman *et al.* 2001; Stamatoyannopoulos *et al.* 2009; Lang and Murray 2011; Drier *et al.* 2013). Possible explanations include accumulation of damage prone ssDNA in late replicating regions (Stamatoyannopoulos *et al.* 2009) or may relate to the fact that some translesion polymerases are not expressed until late in S phase (Waters and Walker 2006). It has been suggested that late in replication error-prone translesion synthesis becomes more important to complete replication of DNA associated with stalled replisomes (Lang and Murray 2011). These observations support the notion that late replicating regions may be sensitized sites that are revealed in certain mutator allele genetic backgrounds.

Increases in mutation clustering and region-specific mutation rates

Mutation clustering may arise due to the coordination of mutational events or as part of hotspots of mutation. It has been observed that yeast cells accumulate clusters of mutations when treated with the DNA alkylating chemical MMS and that tumor cells accumulate clusters of mutations in a variety of contexts, some related to the action of cytosine deaminases (Nik-Zainal *et al.* 2012; Roberts *et al.* 2012; Burns *et al.* 2013). However, the contribution of mutator alleles to these phenomena has not been widely assessed.

We defined 28 mutation clusters across the 68 evolved genomes that were unlikely to have arisen by chance ($P < 9.7 \times 10^{-5}$) using the criteria laid out in the literature for MMS-induced mutation clusters, namely, any two or more SNV, indel, or complex mutations within 100 kb of each other that meet our significance threshold (Roberts *et al.* 2012). WT, *mcm7-ts*, and *pol2-12* did not produce any clusters, while the other mutator genomes contained between one and nine mutation clusters (Figure S1 and Table S6). Typically clusters contained two to three mutations but there were examples of larger clusters in *pol1-ts*, *stn1-13*, and *mas1-1* (Figure S1). Significantly clustered mutations

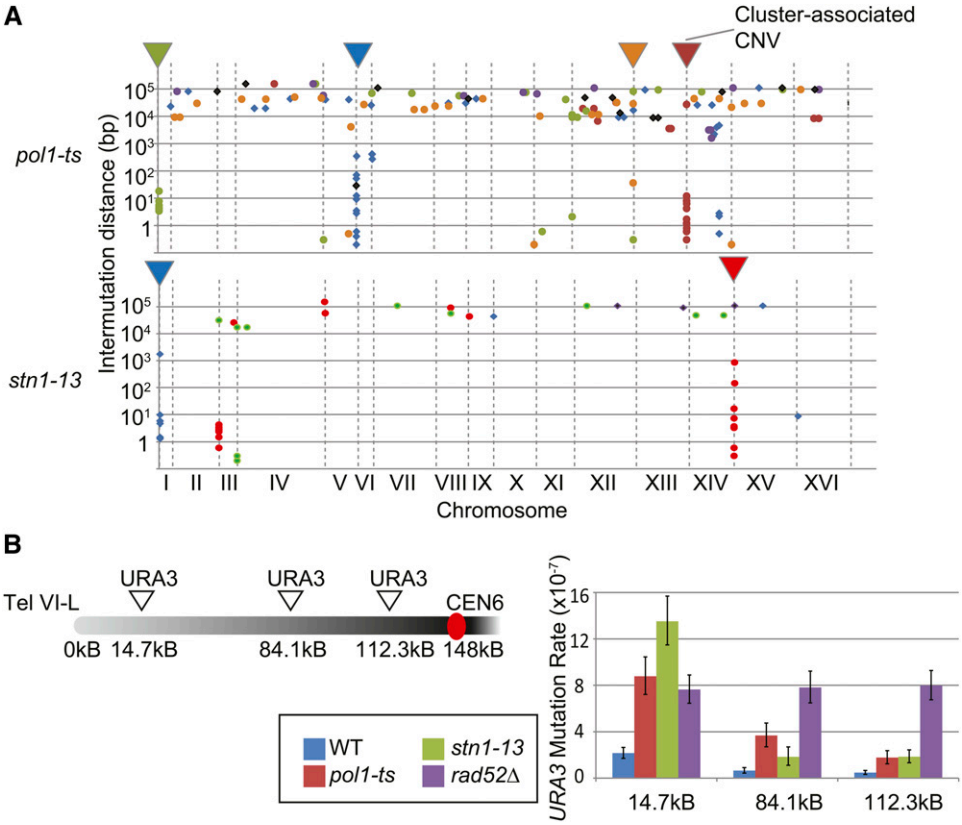

Figure 5 Allele-specific mutation clustering behavior and locus-specific mutation rates. (A) Rainfall plot analysis of mutations in *pol1-ts* and *stn1-13*. Mutations from unique isolates are colored differently. Arrowheads indicate CNVs adjacent to mutation clusters and vertical dotted lines indicate chromosome ends. (B) Mutation rates vary based on position and mutator allele genotype. Left, schematic of chr VI-L noting the three positions at which *URA3* was inserted. Right, the *URA3* mutation rate at each position. Error bars indicate a 95% confidence interval.

spanned as few as 21 bp and as many as 126 kb, with a median of ~3.6 kb (Figure S1). One candidate mechanism for mutation clustering in the absence of genotoxins or APOBECs, is exposure of resected ssDNA during prolonged repair reactions. Local mutation rates increase in this scenario and we found that at least *pol1-ts* and *stn1-13* have an increased frequency of DNA breaks as measured by Rad52 foci (Figure 3C) (Hicks *et al.* 2010; Nik-Zainal *et al.* 2012; Roberts *et al.* 2012; Stirling *et al.* 2012). In support of this model, for nearly all clusters, the mutation density fell within the range of expected resection length for repair of a DNA double-strand break (*i.e.*, up to ~10 kb) (Chung *et al.* 2010).

To examine cluster position, we generated rainfall plots (Nik-Zainal *et al.* 2012). Strikingly, clusters of mutations in *stn1-13* and *pol1-ts* strains occurred almost exclusively in subtelomeric regions, suggesting that the observed telomeric bias may relate to clusters (Figure 5A). At least for *STN1*, this observation supports literature showing that uncapped telomeres lead to hypermutability in association with ssDNA and that *stn1-13* accumulates ssDNA in telomeres (Grandin *et al.* 1997; Yang *et al.* 2008). It is notable that some clusters in *mas1-1* or *rfc2-1* were near repetitive sequences known to be recombination hotspots (*e.g.*, Ty elements, *ENA1,2,5* gene cluster) that may be more likely to initiate inappropriate repair reactions involving resection (Table S6) (St Charles and Petes 2013). Alternatively, many of these clusters occurred adjacent to predicted CNVs (Figure 5A), suggesting that, as in other systems, break-associated mutation clustering might be driving the observed pattern (Hicks *et al.* 2010; Deem *et al.* 2011; Roberts *et al.* 2012; Drier *et al.* 2013). Indeed, break-induced replication itself has been found to be highly error prone and could contribute to clustering in the mutator genomes (Deem *et al.* 2011).

Overall, mutation accumulation and sequencing suggested that local mutation rates were likely higher in subtelomeres for *pol1-ts* and *stn1-13* strains. While we did not observe a subtelomeric bias for mutations in other strains, providing the essential control for the specificity of this observation to *pol1-ts* and *stn1-13*, subtelomeres do exhibit lower variant scores due to their repetitive nature. Moreover, we could not determine whether the primary subtelomeric sequence or the chromosomal context itself was driving mutations. Therefore, we directly tested mutation position biases by introducing the counterselectable *URA3* marker into a subset of mutator lines at loci increasing in distance from the Tel VI-L (Figure 5B). This system enabled us to measure the mutation rate at the same target sequence, *URA3*, in different chromosomal contexts (Lang and Murray 2011). Fluctuation analysis of *URA3* positioned at 15, 84, or 112 kb from Tel VI-L showed dramatic distance-associated decreases in mutation rate for *stn1-13* and *pol1-ts* but not for the *rad52*Δ strain, which showed an identical rate regardless of the marker position (Figure 5B). The presence of mutation prone subtelomeres in *STN1* and *POL1* mutants is consistent with the function of *STN1* in telomere protection and in recruitment of the POLα–primase complexes to subtelomeres for efficient replication (Yang *et al.* 2008; Wang *et al.* 2012).

Conclusion

We identified dozens of essential mutator genes which contribute to a catalog of mutator alleles that define an expanded suite of such cellular mechanisms that suppress mutations. In addition, this work takes a powerful approach to defining mutation spectra for mutator alleles: whole-genome sequencing. These data suggest that mutational signatures vary in an allele-specific fashion and are influenced by several key features: (1) concurrent chromosome instability related to increases in recombination; (2) replication timing, chromosomal context; and (3) break-associated mutation clustering.

Building on this work, and the existing literature on mutator allele-driven mutation signatures (*e.g.*, mismatch repair, DNA polymerase δ) (Larrea *et al.* 2010; Zanders *et al.* 2010), will require both broader studies of more mutator conditions (*e.g.*, genotypes, environment, ploidy) to identify novel signatures, and deeper analysis of larger numbers of variants for a single mutator to improve statistical power. These analyses will be important because tumors are almost certainly influenced by the interaction between specific early genome destabilizing mutations or genotoxins and correspondingly sensitized loci within the genome. In addition to increasing the rate of mutation, mutator alleles introduce base substitution biases or broader locus-associated biases including mutation clustering. Recent detailed analysis of mutation patterns across 21 breast tumors revealed mutation clusters associated with a mutational process termed "kataegis" that is associated with cytosine deamination by APOBEC family proteins (Nik-Zainal *et al.* 2012; Taylor *et al.* 2013). Our data demonstrate that specific mutator genotypes are sufficient to generate mutation clusters in the absence of genotoxins or APOBECs, probably via break-associated hypermutability as seen in models and in human cancers (Roberts *et al.* 2012; Drier *et al.* 2013). Expanding mutation pattern studies in model systems may therefore be key to mechanistically connect specific predisposing genotypes to aspects of mutational signatures seen in tumor genomes.

Acknowledgments

We thank Andrew Murray for strains, Andres Aguilera for plasmids, Greg Lang for help with accessing data, Jessica McLellan for technical assistance, and Samuel Aparicio and members of the Hieter lab for helpful comments. P.C.S. is supported by the Cancer Research Society and was previously a fellow of the Terry Fox Foundation (no. 700044) and the Michael Smith Foundation for Health Research. P.H. acknowledges the National Institutes of Health and the Canadian Institutes of Health Research.

Literature Cited

Alexandrov, L. B., S. Nik-Zainal, D. C. Wedge, P. J. Campbell, and M. R. Stratton, 2013a Deciphering signatures of mutational processes operative in human cancer. Cell. Rep. 3: 246–259.

Alexandrov, L. B., S. Nik-Zainal, D. C. Wedge, S. A. Aparicio, S. Behjati *et al.*, 2013b Signatures of mutational processes in human cancer. Nature 500: 415–421.

Ben-Aroya, S., C. Coombes, T. Kwok, K. A. O'Donnell, J. D. Boeke *et al.*, 2008 Toward a comprehensive temperature-sensitive mutant repository of the essential genes of Saccharomyces cerevisiae. Mol. Cell 30: 248–258.

Breslow, D. K., D. M. Cameron, S. R. Collins, M. Schuldiner, J. Stewart-Ornstein *et al.*, 2008 A comprehensive strategy enabling high-resolution functional analysis of the yeast genome. Nat. Methods 5: 711–718.

Burns, M. B., L. Lackey, M. A. Carpenter, A. Rathore, A. M. Land *et al.*, 2013 APOBEC3B is an enzymatic source of mutation in breast cancer. Nature 494: 366–370.

Cheung, I., M. Schertzer, A. Rose, and P. M. Lansdorp, 2002 Disruption of dog-1 in Caenorhabditis elegans triggers deletions upstream of guanine-rich DNA. Nat. Genet. 31: 405–409.

Chung, W. H., Z. Zhu, A. Papusha, A. Malkova, and G. Ira, 2010 Defective resection at DNA double-strand breaks leads to de novo telomere formation and enhances gene targeting. PLoS Genet. 6: e1000948.

Cingolani, P., and A. Platts, L. L. Wang, M. Coon, T. Nguyen *et al*, 2012 A program for annotating and predicting the effects of single nucleotide polymorphisms, SnpEff: SNPs in the genome of Drosophila melanogaster strain w1118; iso-2; iso-3. Fly (Austin) 6: 80–92.

Couce, A., J. R. Guelfo, and J. Blazquez, 2013 Mutational spectrum drives the rise of mutator bacteria. PLoS Genet. 9: e1003167.

Deem, A., A. Keszthelyi, T. Blackgrove, A. Vayl, B. Coffey *et al.*, 2011 Break-induced replication is highly inaccurate. PLoS Biol. 9: e1000594.

Drier, Y., M. S. Lawrence, S. L. Carter, C. Stewart, S. B. Gabriel *et al.*, 2013 Somatic rearrangements across cancer reveal classes of samples with distinct patterns of DNA breakage and rearrangement-induced hypermutability. Genome Res. 23: 228–235.

Flicek, P., I. Ahmed, M. R. Amode, D. Barrell, K. Beal *et al.*, 2013 Ensembl 2013. Nucleic Acids Res. 41: D48–D55.

Grandin, N., S. I. Reed, and M. Charbonneau, 1997 Stn1, a new Saccharomyces cerevisiae protein, is implicated in telomere size regulation in association with Cdc13. Genes Dev. 11: 512–527.

Hall, B. M., C. X. Ma, P. Liang, and K. K. Singh, 2009 Fluctuation analysis CalculatOR: a web tool for the determination of mutation rate using luria-delbruck fluctuation analysis. Bioinformatics 25: 1564–1565.

Hanahan, D., and R. A. Weinberg, 2011 Hallmarks of cancer: the next generation. Cell 144: 646–674.

Hicks, W. M., M. Kim, and J. E. Haber, 2010 Increased mutagenesis and unique mutation signature associated with mitotic gene conversion. Science 329: 82–85.

Huang, M. E., and R. D. Kolodner, 2005 A biological network in Saccharomyces cerevisiae prevents the deleterious effects of endogenous oxidative DNA damage. Mol. Cell 17: 709–720.

Huang, M. E., A. G. Rio, A. Nicolas, and R. D. Kolodner, 2003 A genomewide screen in Saccharomyces cerevisiae for genes that suppress the accumulation of mutations. Proc. Natl. Acad. Sci. USA 100: 11529–11534.

Jones, S. J., J. Laskin, Y. Y. Li, and O. L. Griffith, J. An *et al*, 2010 Evolution of an adenocarcinoma in response to selection by targeted kinase inhibitors. Genome Biol. 11: R82.

Lada, A. G., A. Dhar, R. J. Boissy, M. Hirano, A. A. Rubel *et al.*, 2012 AID/APOBEC cytosine deaminase induces genome-wide kataegis. Biol. Direct 7: 47; discussion 47.

Lang, G. I., and A. W. Murray, 2008 Estimating the per-base-pair mutation rate in the yeast Saccharomyces cerevisiae. Genetics 178: 67–82.

Lang, G. I., and A. W. Murray, 2011 Mutation rates across budding yeast chromosome VI are correlated with replication timing. Genome Biol. Evol. 3: 799–811.

Lang, G. I., D. P. Rice, M. J. Hickman, E. Sodergren, G. M. Weinstock *et al.*, 2013 Pervasive genetic hitchhiking and clonal interference in forty evolving yeast populations. Nature 500: 571–574.

Larrea, A. A., S. A. Lujan, S. A. Nick McElhinny, P. A. Mieczkowski, M. A. Resnick *et al.*, 2010 Genome-wide model for the normal eukaryotic DNA replication fork. Proc. Natl. Acad. Sci. USA 107: 17674–17679.

Li, H., and R. Durbin, 2009 Fast and accurate short read alignment with Burrows-Wheeler transform. Bioinformatics 25: 1754–1760.

Li, H., B. Handsaker, A. Wysoker, T. Fennell, J. Ruan *et al.*, 2009 The sequence Alignment/Map format and SAMtools. Bioinformatics 25: 2078–2079.

Li, Z., F. J. Vizeacoumar, S. Bahr, J. Li, J. Warringer *et al.*, 2011 Systematic exploration of essential yeast gene function with temperature-sensitive mutants. Nat. Biotechnol. 29: 361–367.

Loeb, L. A., 2011 Human cancers express mutator phenotypes: origin, consequences and targeting. Nat. Rev. Cancer 11: 450–457.

Lynch, M., W. Sung, K. Morris, N. Coffey, C. R. Landry *et al.*, 2008 A genome-wide view of the spectrum of spontaneous mutations in yeast. Proc. Natl. Acad. Sci. USA 105: 9272–9277.

Ma, X., M. V. Rogacheva, K. T. Nishant, S. Zanders, C. D. Bustamante *et al.*, 2012 Mutation hot spots in yeast caused by long-range clustering of homopolymeric sequences. Cell. Rep. 1: 36–42.

Mortensen, U. H., M. Lisby, and R. Rothstein, 2009 Rad52. Curr. Biol. 19: R676–R677.

Nik-Zainal, S., L. B. Alexandrov, D. C. Wedge, P. Van Loo, C. D. Greenman *et al.*, 2012 Mutational processes molding the genomes of 21 breast cancers. Cell 149: 979–993.

Nishant, K. T., N. D. Singh, and E. Alani, 2009 Genomic mutation rates: what high-throughput methods can tell us. Bioessays 31: 912–920.

Nishant, K. T., W. Wei, E. Mancera, J. L. Argueso, A. Schlattl *et al.*, 2010 The baker's yeast diploid genome is remarkably stable in vegetative growth and meiosis. PLoS Genet. 6: 1001109.

Pleasance, E. D., R. K. Cheetham, P. J. Stephens, D. J. McBride, S. J. Humphray *et al.*, 2010a A comprehensive catalogue of somatic mutations from a human cancer genome. Nature 463: 191–196.

Pleasance, E. D., P. J. Stephens, S. O'Meara, D. J. McBride, A. Meynert *et al.*, 2010b A small-cell lung cancer genome with complex signatures of tobacco exposure. Nature 463: 184–190.

Raghuraman, M. K., E. A. Winzeler, D. Collingwood, S. Hunt, L. Wodicka *et al.*, 2001 Replication dynamics of the yeast genome. Science 294: 115–121.

Ragu, S., G. Faye, I. Iraqui, A. Masurel-Heneman, R. D. Kolodner *et al.*, 2007 Oxygen metabolism and reactive oxygen species cause chromosomal rearrangements and cell death. Proc. Natl. Acad. Sci. USA 104: 9747–9752.

Roberts, S. A., J. Sterling, C. Thompson, S. Harris, D. Mav *et al.*, 2012 Clustered mutations in yeast and in human cancers can arise from damaged long single-strand DNA regions. Mol. Cell 46: 424–435.

Shah, S. P., X. Xuan, R. J. DeLeeuw, M. Khojasteh, W. L. Lam *et al.*, 2006 Integrating copy number polymorphisms into array CGH analysis using a robust HMM. Bioinformatics 22: e431–e439.

Smith, S., J. Y. Hwang, S. Banerjee, A. Majeed, A. Gupta *et al.*, 2004 Mutator genes for suppression of gross chromosomal rearrangements identified by a genome-wide screening in Saccharomyces cerevisiae. Proc. Natl. Acad. Sci. USA 101: 9039–9044.

St Charles, J., and T. D. Petes, 2013 High-resolution mapping of spontaneous mitotic recombination hotspots on the 1.1 mb arm of yeast chromosome IV. PLoS Genet. 9: e1003434.

Stamatoyannopoulos, J. A., I. Adzhubei, R. E. Thurman, G. V. Kryukov, S. M. Mirkin *et al.*, 2009 Human mutation rate associated with DNA replication timing. Nat. Genet. 41: 393–395.

Stewart, J. A., F. Wang, M. F. Chaiken, C. Kasbek, P. D. Chastain, 2nd *et al.*, 2012 Human CST promotes telomere duplex replication and general replication restart after fork stalling. EMBO J. 31: 3537–3549.

Stirling, P. C., M. S. Bloom, T. Solanki-Patil, S. Smith, P. Sipahimalani *et al.*, 2011 The complete spectrum of yeast chromosome instability genes identifies candidate CIN cancer genes and functional roles for ASTRA complex components. PLoS Genet. 7: e1002057.

Stirling, P. C., Y. A. Chan, S. W. Minaker, M. J. Aristizabal, I. Barrett *et al.*, 2012 R-loop-mediated genome instability in mRNA cleavage and polyadenylation mutants. Genes Dev. 26: 163–175.

Stratton, M. R., P. J. Campbell, and P. A. Futreal, 2009 The cancer genome. Nature 458: 719–724.

Taylor, B. J., S. Nik-Zainal, Y. L. Wu, L. A. Stebbings, K. Raine *et al.*, 2013 DNA deaminases induce break-associated mutation showers with implication of APOBEC3B and 3A in breast cancer kataegis. Elife 2: e00534.

Veatch, J. R., M. A. McMurray, Z. W. Nelson, and D. E. Gottschling, 2009 Mitochondrial dysfunction leads to nuclear genome instability via an iron-sulfur cluster defect. Cell 137: 1247–1258.

Wang, F., J. A. Stewart, C. Kasbek, Y. Zhao, W. E. Wright *et al.*, 2012 Human CST has independent functions during telomere duplex replication and C-strand fill-in. Cell Rep. 2: 1096–1103.

Waters, L. S., and G. C. Walker, 2006 The critical mutagenic translesion DNA polymerase Rev1 is highly expressed during G(2)/M phase rather than S phase. Proc. Natl. Acad. Sci. USA 103: 8971–8976.

Yang, Y., J. Sterling, F. Storici, M. A. Resnick, and D. A. Gordenin, 2008 Hypermutability of damaged single-strand DNA formed at double-strand breaks and uncapped telomeres in yeast Saccharomyces cerevisiae. PLoS Genet. 4: e1000264.

Zanders, S., X. Ma, A. Roychoudhury, R. D. Hernandez, A. Demogines *et al.*, 2010 Detection of heterozygous mutations in the genome of mismatch repair defective diploid yeast using a Bayesian approach. Genetics 186: 493–503.

Communicating editor: N. Hollingsworth

GENETICS

Supporting Information
http://www.genetics.org/lookup/suppl/doi:10.1534/genetics.113.159806/-/DC1

Genome Destabilizing Mutator Alleles Drive Specific Mutational Trajectories in *Saccharomyces cerevisiae*

Peter C. Stirling, Yaoqing Shen, Richard Corbett, Steven J. M. Jones, and Philip Hieter

DOI: 10.1534/genetics.113.159806

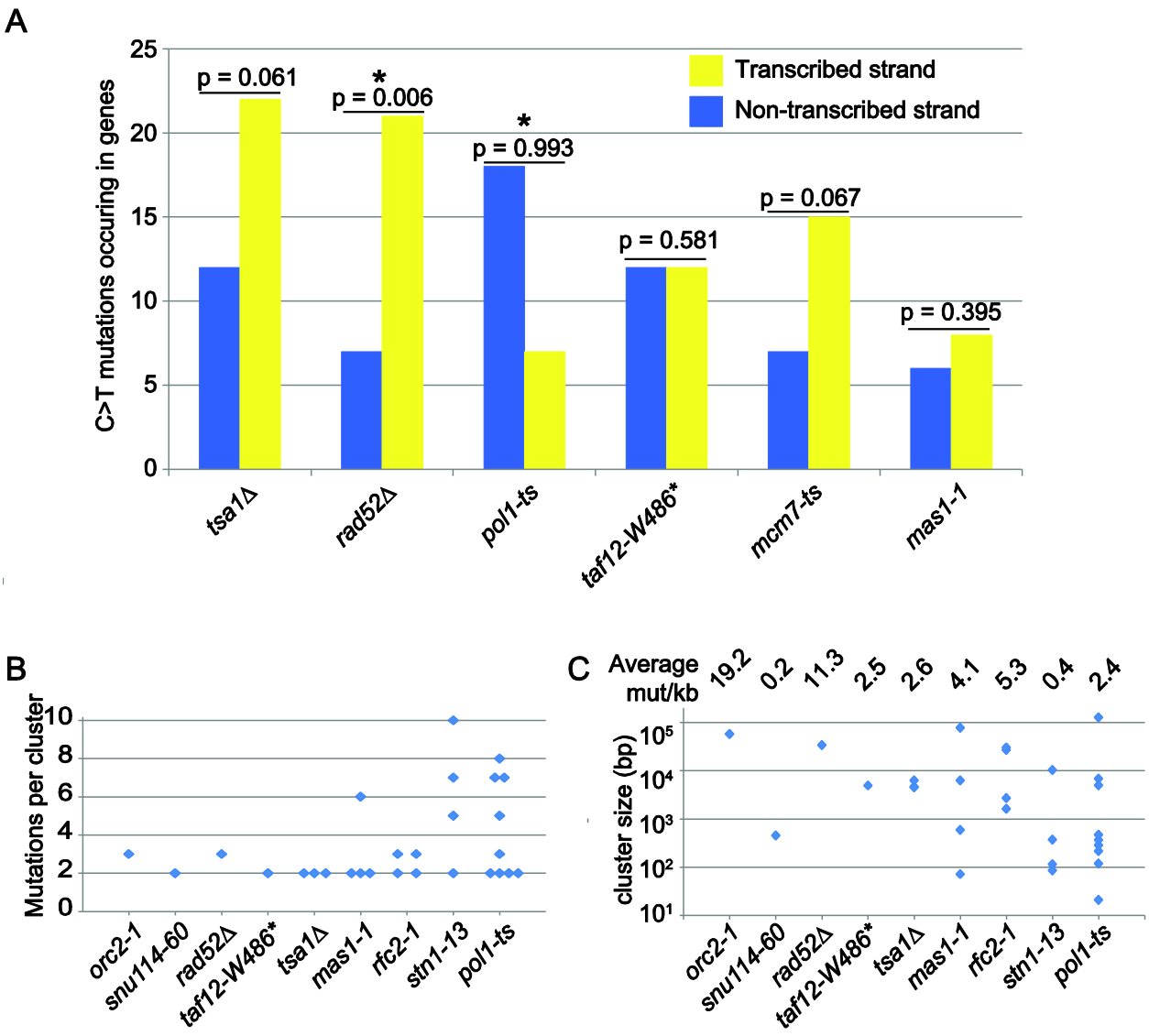

Figure S1 Strand mutational bias and mutation clustering. (A) Shown are C>T mutations, the dominant mutation type, occurring in genes for the six most mutated alleles (i.e. >50 SNVs detected in transcribed regions). The binomial probability, after Holm-Bonferroni correction, that more C>T mutations occur on the non-transcribed strand is shown above the data for each allele. *indicates that *rad52*Δ has a bias toward C>T on the transcribed strand ($p<0.05$) and that *pol1-ts* has a bias toward C>T on the non-transcribed stand ($p>0.95$). (B) Mutations per significant cluster for each allele. (C) Mutation cluster size. Shown on a log scale with the average mutations/kb noted above.

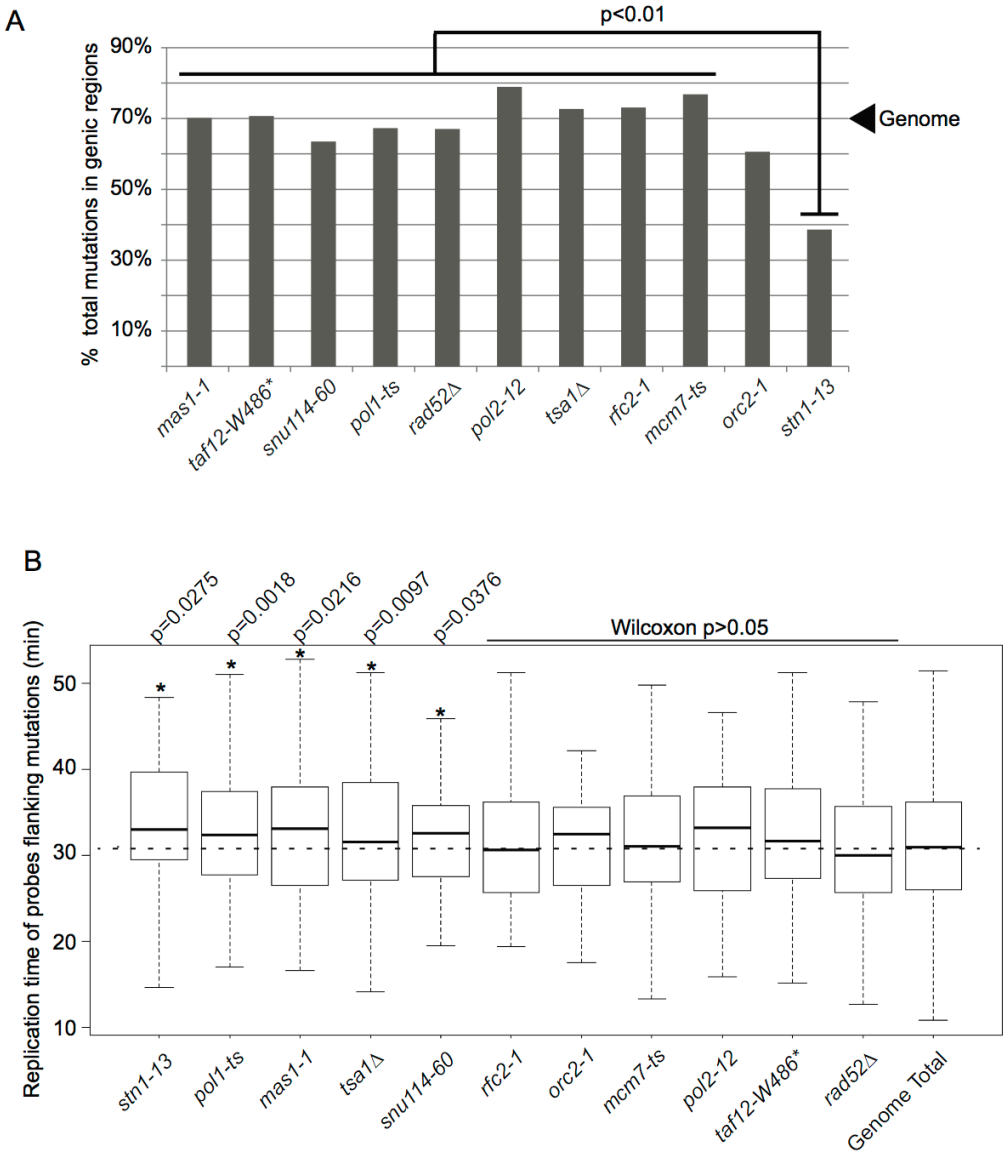

Figure S2 Genomic properties of mutated regions. (A) Proportion of mutations occurring in genes versus intergenic regions. A significant decrease (Fisher test p<0.01) of mutations in genes is seen in *stn1-13*. (B) Replication times flanking detected mutations are from (Raghuraman *et al*. 2001). Wilcoxon ranksum test p-values compared to the genome average are indicated above. The dotted line transecting the boxplots indicate the median time of the genome. Boxplots were produced in R. The black line indicates the median value, the box boundaries indicate the 1st and 3rd quartile and the whiskers indicate 1.5x the interquartile range.

Table S1 Compiled list of yeast mutator alleles. This list includes essential mutators identified in our study, the results of the genome-wide screen for non-essential mutator alleles (Huang et al., 2003) and the compilation of literature reported phenotypes compiled at www.yeastgenome.org.

ORF ID	Gene	Source	Rad52 foci	CIN phenotype*	Group
YIL150C	MCM10	This study	van Pel et al., 2013	GCR, ALF	DNA replication
YBR202W	MCM7	This study	None reported	MCM, Chromosome Loss	DNA replication
YBR060C	ORC2	This study	None reported	CTF x2, GCR x4	DNA replication
YNL261W	ORC5	This study	None reported	CTF	DNA replication
YBL035C	POL12	This study	None reported	GCR	DNA replication
YOL146W	PSF3	This study	van Pel et al., 2013	GCR	DNA replication
YJL194W	CDC6	This study	Stirling et al., 2012	CTF, GCR, ALF	DNA replication
YBL023C	MCM2	This study	Stirling et al., 2012	CTF, GCR	DNA replication
YLR274W	MCM5	This study	Stirling et al., 2012	CTF, chromosome loss, GCR	DNA replication
YML065W	ORC1	This study	Stirling et al., 2012	CTF, ALF	DNA replication
YGL113W	SLD3	This study	Stirling et al., 2012	CTF	DNA replication
YOL094C	RFC4	This study	This study	GCR, ALF	DNA replication AND repair
YJL173C	RFA3	This study	This study	None reported	DNA replication AND repair
YNL262W	POL2	This study	This study	None reported	DNA replication AND repair
YJR006W	POL31	This study	Stirling et al., 2012	CTF, ALF	DNA replication AND repair
YNL102W	POL1	This study	Stirling et al., 2012	CTF x2, GCR	DNA replication AND repair
YJR068W	RFC2	This study	Stirling et al., 2012	CTF, CTF(o/e), GCR	DNA replication AND repair
YDL164C	CDC9	This study	Stirling et al., 2012	GCR, ALF	DNA replication AND repair
YDR062W	LCB2	This study	None reported	None reported	Miscellaneous
YOL144W	NOP8	This study	None reported	None reported	Miscellaneous
YIL118W	RHO3	This study	None reported	None reported	Miscellaneous
YGL098W	USE1	This study	None reported	None reported	Miscellaneous
YMR308C	PSE1	This study	None reported	CTF, GCR	Oxidative Stress / Mito
YLR163C	MAS1	This study	None reported	GCR	Oxidative Stress / Mito
YDL120W	YFH1	This study	None reported	None reported	Oxidative Stress / Mito
YER012W	PRE1	This study	None reported	CTF, CTF(o/e), ALF	Proteolysis
YKL210W	UBA1	This study	None reported	None reported	Proteolysis
YDR082W	STN1	This study	This study	None reported	Telomere ssDNA caps
YGL169W	SUA5	This study	None reported	None reported	Telomere ssDNA caps
YLR010C	TEN1	This study	None reported	None reported	Telomere ssDNA caps
YKL173W	SNU114	This study	None reported	CTF, GCR	Transcription
YGR274C	TAF1	This study	None reported	CTF, GCR	Transcription

YDR145W	TAF12	This study	This study	None reported	Transcription
YMR005W	TAF4	This study	None reported	None reported	Transcription
YLR115W	CFT2	This study	Stirling et al., 2012	GCR, CTF	Transcription
YBR088C	POL30	This study / www.yeastgenome.org	None reported	CTF, ALF	DNA replication AND repair
YDL102W	POL3	This study / www.yeastgenome.org	Stirling et al., 2012	CTF x2, GCR	DNA replication AND repair
YML032C	RAD52	Huang et al., 2003	None reported	CTF, BiM, ALF	DNA repair
YMR224C	MRE11	Huang et al., 2003	None reported	CTF, BiMx2, ALF	DNA repair
YHR120W	MSH1	Huang et al., 2003	None reported	None reported	DNA repair
YML060W	OGG1	Huang et al., 2003	None reported	None reported	DNA repair
YML061C	PIF1	Huang et al., 2003	None reported	GCR	DNA repair
YNL082W	PMS1	Huang et al., 2003	None reported	None reported	DNA repair
YCR066W	RAD18	Huang et al., 2003	None reported	BiM, ALF, GCR, GCR, LOH	DNA repair
YNL250W	RAD50	Huang et al., 2003	None reported	CTF, BiM, ALF, LOH	DNA repair
YDR078C	SHU2	Huang et al., 2003	None reported	None reported	DNA repair
YLR376C	PSY3	Huang et al., 2003	None reported	None reported	DNA repair
YIL132C	CSM2	Huang et al., 2003	None reported	GCR	DNA repair
YML021C	UNG1	Huang et al., 2003	None reported	None reported	DNA repair
YMR167W	MLH1	Huang et al., 2003	Alvaro et al., 2007	None reported	DNA repair
YKL113C	RAD27	Huang et al., 2003	Alvaro et al., 2007	CTF, BiM, ALF, GCR, LOH	DNA repair
YER095W	RAD51	Huang et al., 2003	Alvaro et al., 2007	BiM, ALF, LOH	DNA repair
YGL163C	RAD54	Huang et al., 2003	Alvaro et al., 2007	CTF, BiM, ALF, LOH	DNA repair
YDR076W	RAD55	Huang et al., 2003	Alvaro et al., 2007	BiM, ALF	DNA repair
YDR004W	RAD57	Huang et al., 2003	Alvaro et al., 2007	BiM, ALF	DNA repair
YOR144C	ELG1	Huang et al., 2003	Alvaro et al., 2007	CTF, BiM, ALF, GCR, LOH	DNA repair
YIL116W	HIS5	Huang et al., 2003	None reported	None reported	Miscellaneous
YDL162C	YDL162C	Huang et al., 2003	None reported	BiM, ALF, GCR	Miscellaneous
YLR154C	RNH203	Huang et al., 2003	None reported	ALF, BiM	Miscellaneous
YMR038C	CCS1	Huang et al., 2003	None reported	None reported	Oxidative Stress / Mito
YJR104C	SOD1	Huang et al., 2003	None reported	None reported	Oxidative Stress / Mito
YHR206W	SKN7	Huang et al., 2003	None reported	LOH	Oxidative Stress / Mito
YMR166C	YMR166C	Huang et al., 2003	None reported	None reported	Oxidative Stress / Mito
YML007W	YAP1	Huang et al., 2003	None reported	None reported	Oxidative Stress / Mito
YML028W	TSA1	Huang et al., 2003	Alvaro et al., 2007	BiM, ALF, GCR	Oxidative Stress / Mito
YPR023C	EAF3	www.yeastgenome.org	None reported	None reported	Chromatin
YDR174W	HMO1	www.yeastgenome.org	None reported	Plasmid loss	Chromatin
YDL042C	SIR2	www.yeastgenome.org	None reported	None reported	Chromatin
YKL114C	APN1	www.yeastgenome.org	None reported	None reported	DNA repair
YBL019W	APN2	www.yeastgenome.org	None reported	None reported	DNA repair

YOL090W	MSH2	www.yeastgenome.org	None reported	None reported	DNA repair
YCR092C	MSH3	www.yeastgenome.org	None reported	None reported	DNA repair
YDR097C	MSH6	www.yeastgenome.org	None reported	None reported	DNA repair
YEL062W	NPR2	www.yeastgenome.org	None reported	None reported	DNA repair
YAL015C	NTG1	www.yeastgenome.org	None reported	None reported	DNA repair
YOL043C	NTG2	www.yeastgenome.org	None reported	None reported	DNA repair
YCR014C	POL4	www.yeastgenome.org	None reported	None reported	DNA repair
YPL022W	RAD1	www.yeastgenome.org	None reported	ALF	DNA repair
YML095C	RAD10	www.yeastgenome.org	None reported	BiMx2, ALF	DNA repair
YBR114W	RAD16	www.yeastgenome.org	None reported	None reported	DNA repair
YGR258C	RAD2	www.yeastgenome.org	None reported	None reported	DNA repair
YJR035W	RAD26	www.yeastgenome.org	None reported	None reported	DNA repair
YDR030C	RAD28	www.yeastgenome.org	None reported	None reported	DNA repair
YER171W	RAD3	www.yeastgenome.org	None reported	None reported	DNA repair
YDR419W	RAD30	www.yeastgenome.org	None reported	None reported	DNA repair
YER162C	RAD4	www.yeastgenome.org	None reported	LOH	DNA repair
YHL006C	SHU1	www.yeastgenome.org	None reported	ALF	DNA repair
YDR092W	UBC13	www.yeastgenome.org	None reported	None reported	DNA repair
YBR223C	TDP1	www.yeastgenome.org	None reported	None reported	DNA repair
YLR135W	SLX4	www.yeastgenome.org	None reported	None reported	DNA repair
YDR440W	DOT1	www.yeastgenome.org	None reported	ALF	DNA repair
YPL024W	RMI1	www.yeastgenome.org	Alvaro et al., 2007	CTFx2, BiM, ALF, GCR	DNA repair
YBR274W	CHK1	www.yeastgenome.org	None reported	GCR	DNA repair
YPL194W	DDC1	www.yeastgenome.org	Alvaro et al., 2007	CTF, BiM, ALF	DNA repair
YOR005C	DNL4	www.yeastgenome.org	None reported	None reported	DNA repair
YDL101C	DUN1	www.yeastgenome.org	None reported	ALF, LOH	DNA repair
YKL032C	IXR1	www.yeastgenome.org	None reported	None reported	DNA repair
YDL200C	MGT1	www.yeastgenome.org	None reported	None reported	DNA repair
YOR368W	RAD17	www.yeastgenome.org	Alvaro et al., 2007	BiM, ALF	DNA repair
YER173W	RAD24	www.yeastgenome.org	None reported	BiM, ALF	DNA repair
YLR032W	RAD5	www.yeastgenome.org	None reported	BiM, ALF, GCR	DNA repair
YDL059C	RAD59	www.yeastgenome.org	Alvaro et al., 2007	BiM, ALF	DNA repair
YDR217C	RAD9	www.yeastgenome.org	None reported	BiM, ALF	DNA repair
YDR369C	XRS2	www.yeastgenome.org	None reported	BiM, ALF, LOH	DNA repair
YPR019W	MCM4	www.yeastgenome.org	None reported	ALF	DNA replication
YBR087W	RFC5	www.yeastgenome.org	None reported	CTF, GCR, ALF	DNA replication
YNL072W	RNH201	www.yeastgenome.org	None reported	BiM, ALF, LOH	DNA replication
YGR180C	RNR4	www.yeastgenome.org	None reported	ALF	DNA replication AND repair
YBR252W	DUT1	www.yeastgenome.org	None reported	None reported	DNA replication AND repair
YKL067W	YNK1	www.yeastgenome.org	None reported	None reported	DNA replication AND repair

YEL019C	MMS21	www.yeastgenome.org	None reported	None reported	DNA replication AND repair
YDR288W	NSE3	www.yeastgenome.org	Stirling et al., 2012	CTF, BiM, ALF	DNA replication AND repair
YMR190C	SGS1	www.yeastgenome.org	Alvaro et al., 2007	BiM, ALF, GCR	DNA replication AND repair
YLR383W	SMC6	www.yeastgenome.org	None reported	GCR, nondisjunction	DNA replication AND repair
YLR234W	TOP3	www.yeastgenome.org	None reported	BiM, ALF, GCR	DNA replication AND repair
YAL040C	CLN3	www.yeastgenome.org	None reported	CTF, ALF	Miscellaneous
YBR278W	DPB3	www.yeastgenome.org	None reported	LOH	Miscellaneous
YDR113C	PDS1	www.yeastgenome.org	None reported	Chromosome missegregation	Miscellaneous
YGL255W	ZRT1	www.yeastgenome.org	None reported	None reported	Miscellaneous
YOR330C	MIP1	www.yeastgenome.org	None reported	None reported	Oxidative Stress / Mitochondria
YPR103W	PRE2	www.yeastgenome.org	None reported	Chromosome loss	Proteolysis
YJL001W	PRE3	www.yeastgenome.org	None reported	GCR	Proteolysis
YBR173C	UMP1	www.yeastgenome.org	None reported	None reported	Proteolysis
YOR157C	PUP1	www.yeastgenome.org	None reported	None reported	Proteolysis
YMR039C	SUB1	www.yeastgenome.org	None reported	None reported	Transcription
YJL127C	SPT10	www.yeastgenome.org	None reported	ALF, BiM	Transcription
YJL115W	ASF1	www.yeastgenome.org	Alvaro et al., 2007	BiM, ALF, LOH	Transcription

*CIN phenotypes defined as: MCM = minichromosome maintenance; ALF = MATa-like faker; BiM = Bimater; CTF = chromosome transmission fidelity; LOH = loss-of-heterozygosity; GCR = gross chromosomal rearrangement.

References

Alvaro, D., Lisby, M. & Rothstein, R. *PLoS Genet.* **3**, e228 (2013).

Huang, M. E., Rio, A. G., Nicolas, A. & Kolodner, R. D. *Proc. Natl. Acad. Sci. U. S. A.* **100**, 11529-11534 (2003).

Stirling, P. C. *et al*. *PLoS Genet.* **7**, e1002057 (2011).

Stirling, P. C. *et al*. *Genes Dev.* **26**, 163-175 (2012).

van Pel, D. M. *et al*. *G3 (Bethesda)* **3**, 273-282 (2013).

Table S2 Average sequence coverage for each mutation accumulation (MA) genome

Library ID	Average coverage	Strain	ID	Type
A21529	70.47965081	mas1 evolved A3 -33	PH_125	MA
A21530	60.87233789	mas1 evolved B3 -34	PH_126	MA
A21531	54.56920917	mas1 evolved C3 -35	PH_127	MA
A21532	43.66662041	mas1 evolved D3 -36	PH_128	MA
A21533	49.92637791	mas1 evolved E3 -37	PH_129	MA
A21534	75.52079405	mas1 evolved G3 -38	PH_130	MA
A21500	48.38892651	mas1-1 start -4	PH_96	Parent
A21545	50.36829555	mcm7 evolved 1-D5 -49	PH_141	MA
A21546	65.33676102	mcm7 evolved 1-E5 - 50	PH_142	MA
A21541	48.77270326	mcm7 evolved 2-A5 -45	PH_137	MA
A21542	67.70084456	mcm7 evolved 2-B5 -46	PH_138	MA
A21544	21.66170081	mcm7 evolved 2-E5 (2) -48	PH_140	MA
A21503	59.43827413	mcm7-ts 1-start -7	PH_99	Parent
A21502	55.42162961	mcm7-ts 2-start -6	PH_98	Parent
A21547	65.12670362	orc2-1 evolved A6 -51	PH_143	MA
A21548	65.82275321	orc2-1 evolved B6 -52	PH_144	MA
A21550	77.03362934	orc2-1 evolved E6 (2) -54	PH_146	MA
A21551	68.78371861	orc2-1 evolved G6 (2) -55	PH_147	MA
A21552	66.6580596	orc2-1 evolved H6 (2) -56	PH_148	MA
A21504	68.55303057	orc2-1 start -8	PH_100	Parent
A21571	78.71104085	pol1-ts evolved A10 -75	PH_167	MA
A21572	48.7945061	pol1-ts evolved B10 -76	PH_168	MA
A21573	62.53451087	pol1-ts evolved C10 -77	PH_169	MA
A21574	57.48445895	pol1-ts evolved D10 -78	PH_170	MA
A21575	57.25541198	pol1-ts evolved E10 -79	PH_171	MA
A21576	53.63426617	pol1-ts evolved F10 -80	PH_172	MA
A21508	50.30710695	pol1-ts start -12	PH_104	Parent
A21565	48.78465966	pol2-12 evolved A9 -69	PH_161	MA
A21567	59.59276947	pol2-12 evolved C9 -71	PH_163	MA
A21568	28.62454106	pol2-12 evolved D9 -72	PH_164	MA
A21569	48.65173271	pol2-12 evolved G9 -73	PH_165	MA
A21570	31.62489223	pol2-12 evolved H9 -74	PH_166	MA
A21507	34.25342304	pol2-12 start -11	PH_103	Parent
A21583	70.22598774	rad52D evolved A12 -87	PH_179	MA
A21584	60.00374115	rad52D evolved B12 -88	PH_180	MA
A21585	71.64434409	rad52D evolved C12 -89	PH_181	MA
A21586	60.06868078	rad52D evolved D12 -90	PH_182	MA
A21587	67.21625902	rad52D evolved E12 -91	PH_183	MA
A21588	66.58819676	rad52D evolved F12 -92	PH_184	MA
A21510	54.49184428	rad52D start -14	PH_106	Parent

A21553	55.87855135	rfc2-1 evolved A7 -57	PH_149	MA
A21554	62.2958519	rfc2-1 evolved B7 -58	PH_150	MA
A21555	43.77071135	rfc2-1 evolved C7 -59	PH_151	MA
A21556	51.57940776	rfc2-1 evolved D7 -60	PH_152	MA
A21558	61.35926783	rfc2-1 evolved H7 -62	PH_154	MA
A21505	53.22563888	rfc2-1 start -9	PH_101	Parent
A21559	61.83213143	snu114-60 evolved A8 -63	PH_155	MA
A21560	76.22786227	snu114-60 evolved B8 (2) -64	PH_156	MA
A21561	75.62629163	snu114-60 evolved C8 (1) -65	PH_157	MA
A21562	53.97748497	snu114-60 evolved E8 -66	PH_158	MA
A21563	56.82287191	snu114-60 evolved F8 -67	PH_159	MA
A21564	64.85522318	snu114-60 evolved H8 (1) -68	PH_160	MA
A21506	47.09060297	snu114-60 start -10	PH_102	Parent
A21528	66.71080839	stn1 evolved 1-G2(2) -32	PH_124	MA
A21523	78.985569	stn1 evolved 2-A2 -27	PH_119	MA
A21524	43.95146387	stn1 evolved 2-B2 -28	PH_120	MA
A21527	37.45304741	stn1 evolved 2-G2(2) -31	PH_123	MA
A21499	31.20172972	stn1-13 1-start -3	PH_95	Parent
A21498	36.66158112	stn1-13 2-start -2	PH_94	Parent
A21535	49.622076	taf12 evolved A4 -39	PH_131	MA
A21536	72.13596281	taf12 evolved B4 -40	PH_132	MA
A21537	62.48621642	taf12 evolved C4 -41	PH_133	MA
A21538	86.62640704	taf12 evolved D4 -42	PH_134	MA
A21539	54.69510295	taf12 evolved E4 -43	PH_135	MA
A21540	54.92883869	taf12 evolved F4 -44	PH_136	MA
A21501	50.42151321	taf12_W486* start -5	PH_97	Parent
A21577	35.0507503	tsa1D evolved A11 -81	PH_173	MA
A21578	57.84830838	tsa1D evolved B11 -82	PH_174	MA
A21579	61.80048215	tsa1D evolved C11 -83	PH_175	MA
A21580	47.00550159	tsa1D evolved D11 -84	PH_176	MA
A21581	73.75593676	tsa1D evolved E11 -85	PH_177	MA
A21582	47.85698427	tsa1D evolved F11 -86	PH_178	MA
A21509	67.50977673	tsa1D start -13	PH_105	Parent
A21517	58.88429461	WT evolved A1 -21	PH_113	MA
A21518	52.58702687	WT evolved B1 -22	PH_114	MA
A21519	54.645945	WT evolved C1 -23	PH_115	MA
A21520	54.15120431	WT evolved D1 -24	PH_116	MA
A21521	58.41025882	WT evolved E1-25	PH_117	MA
A21522	67.32363211	WT evolved F1-26	PH_118	MA
A21497	45.1548396	WT single start -1	PH_93	Parent

Table S3 Summary of mutation accumulation experiment

		WT	*orc2-1*	*pol2-12*	*stn1-13*	*mas1-1*	*taf12-486**	*rad52Δ*	*mcm7-ts*	*rfc2-1*	*snu114-60*	*pol1-ts*	*tsa1Δ*
Mutation accumulation genomes sequenced		6	5	6	4	6	6	6	6	5	6	6	5
SNV	GC change	5	13	42	19	59	58	86	53	27	47	59	81
	AT change	8	9	14	14	32	20	35	22	15	15	39	30
Indel	-1 fs	2	3	3	1	5	3	3	10	5	5	8	2
	+1 fs	0	0	2	1	4	6	6	2	1	0	9	4
	2 - 230 bp	1	1	1	6	1	7	3	2	2	2	8	2
Complex (within 10bp)		0	1	0	4	3	3	0	2	2	3	11	2
Copy number variant	Whole chromosome	0	0	1	2	1	0	0	1	2	0	4	0
	Sub-telomeric	0	0	3	7	2	0	0	0	2	0	11	4
	Segmental	0	0	0	1	0	0	0	0	2	0	6	1
Other Struc. Variant		1	0	1	0	1	1	0	0	4	0	0	0
Total Events detected		17	27	67	55	108	98	133	92	62	72	155	126
Fold increase in WGS mutation		1.00	1.59	3.94	3.24	6.35	5.76	7.82	5.41	3.65	4.24	9.12	7.41
Fold increase in CAN^r		1.00	6.36	16.64	11.48	3.65	7.91	14.74	9.83	5.44	7.72	12.35	12.63
Mutations per genome		2.83	5.40	11.17	13.75	18.00	16.33	22.17	15.33	12.40	12.00	25.83	25.20
Fold increase per genome		1.00	1.91	3.94	4.85	6.35	5.76	7.82	5.41	4.38	4.24	9.12	8.89

Table S4 Details of mutations detected in whole genome sequencing.

*Mutation clusters are labelled in blue highlighting.
**In combination with the strain name, each mutation has a unique ID. Occasionally, a series of large CNVs covering almost an entire chromosome were seen, most likely representing whole chromosome gains. These are numbered consecutively here (e.g. CNV1a, 1b, 1c, etc.) but were treated as single events for our analysis in Table S3.

Table S4 is available for download as an Excel file at http://www.genetics.org/lookup/suppl/doi:10.1534/genetics.113.159806/-/DC1.

Table S5 Analysis of SNV mutation type.

Pooled SNV	*rfc2-1*	*pol1-ts*	*stn1-13*	*rad52Δ*	*snu114-60*	*taf12-W486**	*pol2-12*	*mas1-1*	*mcm7-ts*	*orc2-1*	*tsa1Δ*	WT (Lynch et al., 2008; Lang et al., 2013)
C>A	1	16	5	17	9	14	9	24	16	3	23	503
C>G	10	12	3	29	14	14	16	15	9	3	19	308
T>A	4	16	3	11	4	9	5	7	10	3	8	148
T>G	1	5	0	10	5	5	3	9	5	1	7	118
C>T	16	31	11	40	24	30	17	20	28	7	39	513
T>C	10	18	11	14	6	5	6	16	7	5	15	192
	42	98	33	121	62	77	56	91	75	22	111	1782
Uncorrected p-values	0.0002	0.0036	0.0041	0.0142	0.1220	0.1727	0.2230	0.2630	0.2724	0.3019	0.4768	-
Corrected p-value	**0.0027**	**0.0359**	**0.0373**	0.1135	-	-	-	-	-	-	-	-

Table S6 Details of significant mutation clusters.

Strain	Cluster ID	p-value	Size (bp)	Number of mutations
orc2-1	*orc2-1* cluster 1	1.94E-06	57756	3
snu114-60	*snu114-60* cluster 5	1.04E-07	454	2
*rad52*Δ	*rad52*Δ cluster13	3.90E-05	33842	3
*taf12-W486**	*taf12-W486** cluster 7	2.16E-05	4958	2
*tsa1*Δ	*tsa1*Δ cluster 18	7.83E-05	6264	2
*tsa1*Δ	*tsa1*Δ cluster 20	4.10E-05	4528	2
*tsa1*Δ	*tsa1*Δ cluster 3	4.46E-05	4721	2
stn1-13	*stn1-13* cluster 1	9.24E-42	372	10
stn1-13	*stn1-13* cluster 2	3.42E-09	86	2
stn1-13	*stn1-13* cluster 3	1.63E-18	10291	7
stn1-13	*stn1-13* cluster 4	1.44E-22	115	5
mas1-1	*mas1-1* cluster 13	5.38E-09	72	2
mas1-1	*mas1-1* cluster 14	3.94E-05	6308	2
mas1-1	*mas1-1* cluster 2	3.54E-07	595	2
mas1-1	*mas1-1* cluster 7	2.19E-09	77644	6
rfc2-1	*rfc2-1* cluster 1	8.86E-07	1618	2
rfc2-1	*rfc2-1* cluster 3	2.50E-06	30185	3
rfc2-1	*rfc2-1* cluster 4	1.78E-06	26911	3
rfc2-1	*rfc2-1* cluster 5	2.50E-06	2721	2
pol1-ts	*pol1-ts* cluster 1	1.06E-18	4983	7
pol1-ts	*pol1-ts* cluster 10	8.23E-30	470	8
pol1-ts	*pol1-ts* cluster 11	8.53E-10	21	2
pol1-ts	*pol1-ts* cluster 13	1.41E-07	288	2
pol1-ts	*pol1-ts* cluster 17	2.25E-07	364	2
pol1-ts	*pol1-ts* cluster 2	3.24E-07	6814	3
pol1-ts	*pol1-ts* cluster 4	5.95E-09	126611	7
pol1-ts	*pol1-ts* cluster 5	8.76E-20	216	5
pol1-ts	*pol1-ts* cluster 9	2.49E-08	120	2
	AVERAGE	9.82E-06	14619	4

Table S7 Yeast strains and plasmids used in this study.

Plasmid name	Relevant features	Source
LNA	*LEU2-5'-LEU2-3'*, *TRP1*, CEN	Andres Aguilera (Also used in Stirling et al., 2012)
Strain name	**Relevant genotype**	**Source**
BY4741	MATa *ura3Δ0 leu2Δ0 his3Δ1 met15Δ0*	Open biosystems
ts-alleles (YFEG = any essential gene)	BY4741, *YFEG::KanMX*	Li et al., 2011
DAmP alleles	BY4741 *YFEG-DAmP::KanMX*	Breslow et al., 2008
PSY1090	MATa *ura3Δ0 leu2Δ0 his3Δ1 rad52Δ::KanMX*	This study
PSY1087	MATa *ura3Δ0 leu2Δ0 his3Δ1 tsa1Δ::KanMX*	This study
PSY366	BY4741, *Rad52-YFP::URA3*	Stirling et al., 2012
PSY1111	MATa *can1Δ::STE2pr-SpHis5 lyp1Δ RAD52-YFP::URA3 rfa3-313::KanMX*	Stirling et al., 2012
PSY1137	MATa *can1Δ::STE2pr-SpHis5 lyp1Δ RAD52-YFP::URA3 taf12-W486*::KanMX*	Stirling et al., 2012
PSY1133	MATa *can1Δ::STE2pr-SpHis5 lyp1Δ RAD52-YFP::URA3 pol2-12::KanMX*	Stirling et al., 2012
PSY1110	MATa *can1Δ::STE2pr-SpHis5 lyp1Δ RAD52-YFP::URA3 stn1-13::KanMX*	Stirling et al., 2012
PSY1125	MATa *can1Δ::STE2pr-SpHis5 lyp1Δ RAD52-YFP::URA3 rfc4-20::KanMX*	Stirling et al., 2012
PSY1120	MATa *can1Δ::MFA1pr-HIS3::LEU2 lyp1Δ LYS2 his3Δ1 sld3-ts::URA3 RAD52-YFP::KanMX*	Stirling et al., 2012
GL2	BY4741, *aad6Δ::URA3*	Lang and Murray, 2011
GL15	BY4741, *bst1Δ::URA3*	Lang and Murray, 2011
GL21	BY4741, *hxt10Δ::URA3*	Lang and Murray, 2011
PSY1157	BY4741, *aad6Δ::URA3*, *pol1-ts::KanMX*	This study
PSY1151	BY4741, *bst1Δ::URA3*, *pol1-ts::KanMX*	This study
PSY1153	BY4741, *hxt10Δ::URA3*, *pol1-ts::KanMX*	This study
PSY1167	BY4741, *aad6Δ::URA3*, *stn1-13::KanMX*	This study
PSY1168	BY4741, *bst1Δ::URA3*, *stn1-13::KanMX*	This study
PSY1163	BY4741, *hxt10Δ::URA3*, *stn1-13::KanMX*	This study
PSY1655	BY4741, *aad6Δ::URA3*, *rad52Δ::KanMX*	This study
PSY1656	BY4741, *bst1Δ::URA3*, *rad52Δ::KanMX*	This study
PSY1658	BY4741, *hxt10Δ::URA3*, *rad52Δ::KanMX*	This study

References

Stirling, P.C. *et al. Genes Dev*. **2**, 163-175 (2012).

Lang, G.I. *et al*. *Genome Biol. Evol.* 799-811 (2011).

Li, Z. *et al*. *Nat Biotechnol* **29,** 361-367 (2011).

Breslow D.K. *et al*. *Nat Methods* **5,** 711-718 (2008).